INTERNATIONAL JOURNAL FOR NUMERICAL METHODS IN FLUIDS, VOL. 21, 591–613 (1995)

A CONTROL-VOLUME BASED FINITE ELEMENT METHOD FOR THREE-DIMENSIONAL INCOMPRESSIBLE TURBULENT FLUID FLOW, HEAT TRANSFER, AND RELATED PHENOMENA

V. A. F. COSTA

Departamento de Engenharia Mecânica da Universidade de Aveiro, Campus Universitário de S. Tiago, 3800 Aveiro, Portugal

L. A. OLIVEIRA AND A. R. FIGUEIREDO

Departamento de Engenharia Mecânica da Universidade de Coimbra, Largo D. Dinis, 3000 Coimbra, Portugal

SUMMARY

A control-volume based finite element method of equal-order type for three-dimensional incompressible turbulent fluid flow, heat transfer, and related phenomena is presented. The discretization equations are based mainly on the physics of the phenomena under consideration, more than on mathematical arguments. Special emphasis is devoted to the discretization of the convective terms and the continuity equation, and to the treatment of the boundary conditions imposed by the use of a high Reynolds k-ε type turbulence model. The pressure-velocity coupling in the fluid flow calculation is made from a derivative of the original SIMPLER method, without pressure correction. The discretized equations are solved in a sequential, rather than a coupled, form with significant advantages in the required computer time and storage. The method is an extension of a former version proposed by us for two-dimensional, laminar problems, and is here successfully applied to the following situations: three-dimensional deflected turbulent jet, and flows in 90° and 45° junctions of ducts with rectangular cross sections. The calculated results are in very good agreement with the experimental and numerical (obtained with the well established finite difference method) data available in the literature.

KEY WORDS: three-dimensional flow; control-volume finite element method; mass weighted upwind interpolation; equal-order method; turbulent flow

1. INTRODUCTION

The finite difference method (FDM) and the finite element method (FEM) are two major approaches that are currently used to numerically solve the partial differential equations (PDE) associated with fluid flow, heat transfer, and related phenomena.[1,2] The FDM has been extensively and successfully used to simulate a large variety of problems, but its inherent simplicity is degraded when the domain geometry is not close to the most conventional orthogonal co-ordinate systems. The geometric details of the calculation domain do not affect the simplicity of the FEM, and the capability of easily dealing with complex geometries without additional difficulties is one of the major advantages of this family of methods.

The usual practice in the FEM is to follow the conventional weighted residuals or variational approaches to obtain the discrete analogue of the partial differential equations.[3] In this work, the control volume based approach is followed with its well known advantages.[4] The CVFEM presented here is the result of a study of the works of Baliga,[5] Baliga and Patankar,[6,7,8] Prakash and Patankar,[9] Prakash,[10] Hookey,[11] Schneider,[4] and Saabas.[12] The implementation of the method of Saabas[12,13] is followed with some modifications.

CCC 0271–2091/95/070591–23

Received August 1994
Revised March 1995

A very complete summary of the CVFEM developed by Baliga and Patankar,[5,6,7] including the modifications proposed by Prakash[10] and Hookey[11] is presented by Baliga and Patankar.[8] These methods have the common characteristic of using a shape function which is exponential in the mean flow direction and linear in the directions normal to it. A major shortcoming is that negative coefficients can arise in the discretization equations, with the subsequent inherent problems.[14] Additional difficulties are experienced by the CVFEMs proposed Prakash[10] and Hookey,[11] especially in problems with open domains, where inflows and outflows occur. These difficulties were experienced in a preliminary phase of this work, and they have been discussed in detail by Saabas.[12]

In incompressible flow problems the pressure distribution is implicitly governed by the momentum and the continuity equations, and special care is needed to avoid the possibility of physically unrealistic checkerboard-type pressure distributions. If the source term is not considered in the shape function,[5,6,7] it is necessary to use a so-called unequal-order method. However, a co-located equal-order method, in which all the variables are computed at the same grid points in the domain, has been proposed by Prakash and Patankar.[9]

The above mentioned difficultues can be overcome if the following practice is adopted: (i) the diffusive fluxes are computed assuming a linear profile in the three coordinate directions over each element; (ii) the convective fluxes are computed from the mass-weighted skewed upwinding procedure of Schneider and Raw,[4,15] which is adapted to the form of the present finite-elements; and (iii) the equal-order method proposed by Prakash and Patankar[9] is followed to obtain a suitable discretization equation for the pressure. This is esssentially the procedure followed by Costa and Oliveira[1] and Saabas[12], and discussed in recent papers by Masson *et al.*[16] and Saabas and Baliga.[17,18] The ingredients used in the present work are essentially those used by Saabas[12], but there are some novelties in the derivation and presentation of the method. Additionally, the source terms are treated in a different way, as well as the boundary conditions associated with the used turbulence model.

The advantages and disadvantages of the proposed method over the standard ones are: (i) the physical meaning and the conservative characteristics of the whole method, which is not the usual practice within the finite element methods; (ii) the use of the control-volume formulation together with finite elements, which have the capability of easily working with domains of complex geometry, is a great advantage over the well established control-volume finite difference methods; and (iii) the used segregated approach in the context of finite element methods, which require much less computational resources and time and is more flexible than the usual coupled ones.

The applications presented in order to show the capabilities of the method are devoted to turbulent fluid flow calculations.

2. MATHEMATICAL MODELLING

2.1. The general differential equation

All the PDEs governing the steady three-dimensional turbulent situations involving fluid flow, heat transfer, and related phenomena can be obtained as specific particular cases of the following general differential equation, written in the conservative form and in Cartesian tensor notation, for i ranging from 1 to 3,

$$\frac{\partial}{\partial x_i}(\rho u_i \phi) = \frac{\partial}{\partial x_i}\left(\Gamma_{\text{eff},\phi}\frac{\partial \phi}{\partial x_i}\right) + S_\phi \tag{1}$$

for the time-mean variables. The conservation principles are established for extensive (proportional to the mass m) properties Φ, the ϕ variable in the general differential equation being an intensive (mass independent) property, which is the specific value of Φ, that is, $\phi = \Phi/m$.

Table I. Set of constants used in the high-Reynolds k-ε turbulence model

constant	$C\mu$	σ_k	σ_ε	$C_{1\varepsilon}$	$C_{2\varepsilon}$
value	0·09	1·0	1·3	1·44	1·92

2.2. *Turbulence modelling*

The turbulence transport is simulated by the well known high-Reynolds k-ε turbulence model,[19] in which two additional PDEs must be solved for the variables $k = \overline{u_i' u_i'}/2$, the turbulence kinetic energy per unit mass, and $\varepsilon = (\mu/\rho)\overline{(\partial u_i'/\partial x_j)^2}$, the isotropic rate of dissipation of k, where u_i' is the fluctuating velocity and μ is the dynamic viscosity of the fluid. The turbulent dynamic viscosity, which is a property of the flow, is $\mu_t = C_\mu \rho k^2/\varepsilon$.

As in all turbulence models, the high-Reynolds k-ε turbulence model involves some empirical information. In this work, we use the five empirical constants recommended by Launder and Spalding[20] which are listed in Table I.

2.3. *Boundary conditions imposed by the high-Reynolds k-ε turbulence model*

In turbulent flows, the existence of intense gradients near the wall boundaries requires some special treatment to allow computations with grids that are not very fine near the wall. Here, the viscous regions close to the wall are bridged by the use of well-established wall functions,[20] and the boundary conditions for the near-wall points are determined from suitable relationships which account for the sharp gradients that exist there.

Considering a turbulent boundary layer over a flat plate, and assuming that the shear stress τ_w is constant near the wall, it can be easily shown that the velocity exhibits the $u^+ = \ln(Ey^+)/\chi$ non-dimensional logarithmic profile in the inertial sub-layer. Here, the reference velocity is the friction velocity, $u_\tau = \sqrt{\tau_w/\rho}$, the non-dimensional distance from the wall is the Reynolds number, $y^+ = \rho u_\tau y/\mu$, $\chi = 0{\cdot}42$ is the von Kármán constant, and the E factor, which depends of the wall roughness, can be assumed to be $E = 9{\cdot}8$ for smooth walls.

In the near-wall region, it can be assumed that the production and dissipation of turbulence kinetic energy are in equilibrium, that is, $\mu_t P_k = \rho\varepsilon$. After some manipulation of this reduced form of the k equation, it can be shown that $k = u_\tau^2/\sqrt{C_\mu}$ and $\varepsilon = u_\tau^3/\chi y$ are possible boundary conditions for k and ε, respectively. However, as u_τ is unknown, it is a better practice to express k and ε as functions of only known variables. The introduction of the non-dimensional logarithmic profile and the definition of the friction velocity leads, after some manipulation, to the following expression of τ_w

$$\tau_w = -\lambda_w U_P, \tag{2}$$

where U_P is the velocity component parallel to the wall, and

$$\lambda_w = \frac{\chi^4 \sqrt{c_\mu k^2 \rho}}{\ln(Ey^+)}. \tag{3}$$

The expression of τ_w given by (2), when multiplied by the area over which it acts, is the boundary condition to use in the momentum equations. In general three-dimensional problems τ_w (and U_P) have three non-zero components. Elimination of u_τ through (2) in the above equations then leads to the more suitable expressions for k and ε boundary conditions

$$k = \frac{1}{\sqrt{C_\mu}} \left[\frac{\chi}{\ln(Ey^+)}\right]^2 U_P^2, \tag{4}$$

Table II. ϕ and its corresponding expressions for $\Gamma_{\text{eff},\phi}$ and S_ϕ.

ϕ	$\Gamma_{\text{eff},\phi}$	S_ϕ
1	0	0
u_j	$\mu + \mu_t$	$-\frac{\partial p}{\partial x_j} + \frac{\partial}{\partial x_i}(\mu + \mu_t)\frac{\partial u_i}{\partial x_j} + \rho f_j$
k	$\mu + \mu_t/\sigma_k$	$P_k - \rho\varepsilon$
ε	$\mu + \mu_t/\sigma_\varepsilon$	$(C_{1\varepsilon}P_k - C_{2\varepsilon}\rho\varepsilon)\varepsilon/k$

$$\varepsilon = \frac{(C_\mu k^2)^{3/4}}{\chi y}. \tag{5}$$

An expression for y^+, which is determined from only known varaibles, can also be found as $y^+ = \rho y \sqrt[4]{C_\mu k^2}/\mu$.

The k and ε boundary conditions at the inflow boundaries, where the inlet velocity and the turbulence intensity (defined as $T_i = \sqrt{u_i' u_i'}/3/U_{\text{in}} = \sqrt{2k_{\text{in}}/3}/U_{\text{in}}$) are given, may be expressed by $k_{\text{in}} = (3/2)(T_i U_{\text{in}})^2$ and $\varepsilon = k^{3/2}/l$, were l is the smallest *diameter* possible for the large eddies. Usual values range from $l = 0{\cdot}03L$ to $l = 0{\cdot}15L$, where L is the relevant length of the inflow boundary.

2.4. *Summary of the mathematical modelling*

The particular expressions of $\Gamma_{\text{eff},\phi}$ and S_ϕ for the corresponding specifications of the general dependent variable, ϕ, are presented in Table II, where P_k is the production rate of k by the action of the velocity gradients, given by

$$P_k = \mu_t\left(\frac{\partial u_i}{\partial x_j} + \frac{\partial u_j}{\partial x_i}\right)\frac{\partial u_i}{\partial x_j}. \tag{6}$$

3. INTEGRAL CONSERVATION EQUATION AND DOMAIN DISCETIZATION

3.1. *Integral conservation equation*

The general differential equation (1) can be rewritten in the form

$$\frac{\partial}{\partial x_i}\left(\rho u_i \phi - \Gamma_{\text{eff},\phi}\frac{\partial \phi}{\partial x_i}\right) = S_\phi, \tag{7}$$

where the total (diffusive plus convective) flux components, $J_{\phi,i} = \rho u_i \phi - \Gamma_{\text{eff},\phi}(\partial\phi/\partial x_i)$, in the i direction are identified. Equation (7) can now be written in terms of fluxes as $\partial J_{\phi,i}/\partial x_i = S_\phi$ but, as the left side of this equation is the divergence of the total flux, it becomes

$$\text{div}\mathbf{J}_\phi = S_\phi. \tag{8}$$

Equation (8) needs to be integrated over a control volume, *cv*, to find the ϕ distribution, and this is established as

$$\int_{cs} \mathbf{J}_\phi . \mathbf{n}\, \mathrm{d}S = \int_{cv} S_\phi\, \mathrm{d}V \tag{9}$$

after application of the Gauss divergence theorem on the left hand side, where *cs* is the closed control surface that contains the control volume, *cv*, and $\mathbf{n}$ is the unit outward normal to this control surface. The total flux, $\mathbf{J}_\phi$, can be decomposed in its diffusive and convective components defined, respectively,

as $\mathbf{J}_\phi^D = -\Gamma_{\text{eff},\phi}\nabla\phi = -\Gamma_{\text{eff},\phi}(\partial\phi/\partial x_i)\mathbf{e}_i$ and $\mathbf{J}_\phi^C = \rho\mathbf{V}\phi = \rho u_i\phi\mathbf{e}_i$, where $\mathbf{e}_i$ is the unit vector in the i direction. Finally, for later use, the integral of the general differential equation can be written in the form

$$\int_{cs} \mathbf{J}_\phi^C.\mathbf{n}\, dS + \int_{cs} \mathbf{J}_\phi^D.\mathbf{n}\, dS = \int_{cv} S_\phi\, dV \tag{10}$$

which is the most suitable form to integrate the different contributions (convective, diffusive, and source) for the conservation of Φ over a control volume. As will be seen later, each of these contributions is integrated by a different procedure, the leading reasons being associated with the physics of each particular phenomenon.

3.2. Domain discretization

The domain is divided into four-node tetrahedral elements. For reasons of simplicity and economy, in the present CVFEM, the domain is discretized using a structured grid in which the nodes are distributed along easily identifiable lines, and the number of such lines along a particular direction is the same throughout the whole domain. Following Saabas,[12] to obtain the structured grid, the domain is first discretized into eight node bricks, and each brick is then divided into six four node tetrahedral elements, as sketched in Figure 1. All the dependent variables are stored at these nodes. Due to the planar character of the brick surfaces, irregular boundaries are treated as piecewise-planar surfaces. The division of each brick into six tetrahedral elements should be made with care to ensure a good discretization equation for the pressure at all the nodes; this will be examined further, when discretizing the pressure equation.

After definition of the finite elements, the next step is the construction of the control volumes. This definition differs from that followed by LeDain-Muir and Baliga,[21] and is that proposed by

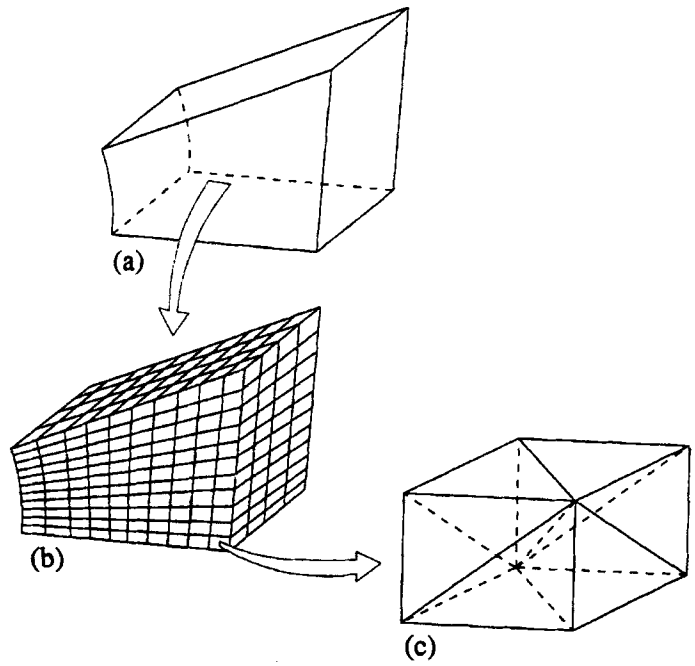

Figure 1. Domain discretization

Saabas,[12,17,18] which is the three-dimensional extension of the discretization suggested by McCormick.[22] The midpoints of the element edges are defined as the points a to f in Figure 2, and these midpoints are then joined to form three plane control sub-surfaces, two of which are triangular and one is quadrilateral.

The area of each of the control sub-surfaces is given by

$$S_1 = |\mathbf{ac} \times \mathbf{af}|/2, S_2 = |\mathbf{fd} \times \mathbf{fc}|, S_3 = |\mathbf{bc} \times \mathbf{be}|/2 \tag{11}$$

and the unit outward normals to each of these control sub-surfaces are

$$\mathbf{n}_1 = (\mathbf{ac} \times \mathbf{af})/|\mathbf{ac} \times \mathbf{af}|, \mathbf{n}_2 = (\mathbf{fd} \times \mathbf{fc})/|\mathbf{fd} \times \mathbf{fc}|, \mathbf{n}_3 = (\mathbf{bc} \times \mathbf{be})/|\mathbf{bc} \times \mathbf{be}|. \tag{12}$$

These three control sub-surfaces define four control sub-volumes in a tetrahedral element, each one associated with a node of the element, and their volumes are

$$V_1 = V_3 = V_e/8, V_2 = V_4 = 3V_e/8, \tag{13}$$

with $V_e = |\Delta|/6$, where Δ is given by

$$\Delta = \sum_{n=1}^{3}(x_{1,n} - x_{1,4})[(x_{2,\langle n+1\rangle} - x_{2,4})(x_{3,\langle n+2\rangle} - x_{3,4}) - (x_{2,\langle n+2\rangle} - x_{2,4})(x_{3,\langle n+1\rangle} - x_{3,4})]. \tag{14}$$

The operator $\langle\ \rangle$ acts over the n and k indices through the expressions $\langle n + k\rangle = n + k$ if $n + k \leqslant 3$ and $\langle n + k\rangle = n + k - 3$ if $n + k > 3$, and $x_{i,n}$ denotes the x_i co-ordinate at the n node.

When the bricks are assembled, the control sub-surfaces and sub-volumes are also assembled to form a closed control surface around each internal node, thus defining a control volume associated with it. To make this assembling possible, the form in which the bricks are divided into six tetrahedral elements must be ordered, defining four different types of bricks. The bricks fill in the domain in a periodic fashion, with the repetition of a set of four (of different type) bricks.

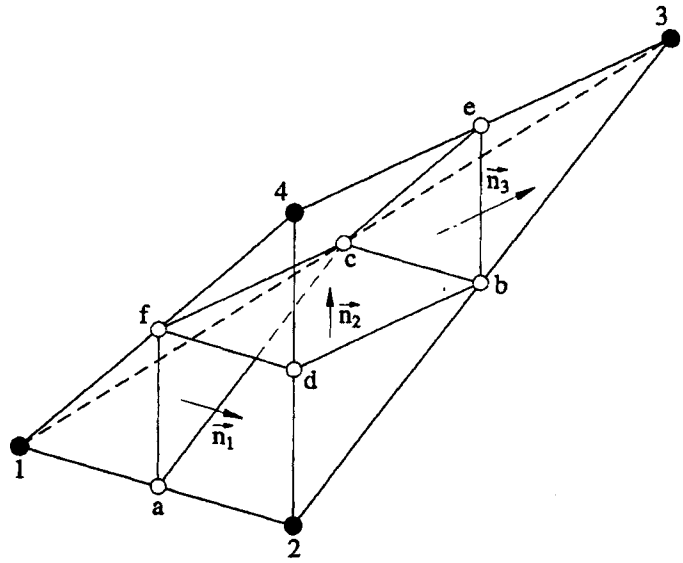

Figure 2. Control sub-volumes and sub-surfaces definitions in a element

4. INTEGRATION OF THE DIFFERENT TERMS OVER THE CONTROL SUB-SURFACES AND SUB-VOLUMES

4.1. Integration of the source term

The source term can be expressed in the following linearized general form[14] $S_\phi = S_{\phi,\mathrm{P}}\phi + S_{\phi,\mathrm{C}}(S_{\phi,\mathrm{P}} \leqslant 0)$. In an element, it is assumed that $S_{\phi,\mathrm{P}}$ and $S_{\phi,\mathrm{C}}$ are associated with each node, that is, in each element $(S_{\phi,\mathrm{C}})_n$ and $(S_{\phi,\mathrm{P}})_n$, $n = 1, 2, 3, 4$, are defined and the linearized general form of S_ϕ becomes

$$(S_\phi)_n = (S_{\phi,\mathrm{C}})_n + (S_{\phi,\mathrm{P}})_n\phi_n \ ((S_{\phi,\mathrm{P}})_n \leqslant 0). \tag{15}$$

The integration of the source term is immediate with the above assumptions to give

$$\int_{V_n} S_\phi \, \mathrm{d}V = (S_{\phi,\mathrm{C}})_n V_n + (S_{\phi,\mathrm{C}})_n V_n \phi_n, \quad n = 1, 2, 3, 4, \tag{16}$$

where the summation convention does not apply.

4.2. Integration of the diffusive flux

The diffusive flux is integrated assuming that ϕ varies linearly with the x_i coordinates in each element, that is

$$\phi = A^i_\phi x_i + A^4_\phi, \tag{17}$$

which is consistent with the elliptical nature of the diffusion phenomenon. As the diffusive flux includes only the first-order partial derivatives of ϕ, the value (or the expression) of A^4_ϕ is irrelevant. In tensor notation, for n ranging from 1 to 4, we can write

$$A^i_\phi = B^i_n \phi_n / \Delta, \tag{18}$$

where Δ is the determinant given by (14). The expressions for the B^i_n coefficients, for $n = 1$, 2 and 3, can be written as

$$B^i_n = (x_{\langle i+1\rangle,\langle n+1\rangle} - x_{\langle i+1\rangle,4})(x_{\langle i+2\rangle,\langle n+2\rangle} - x_{\langle i+2\rangle,4}) - (x_{\langle i+1\rangle,\langle n+2\rangle} - x_{\langle i+1\rangle,4})(x_{\langle i+2\rangle,\langle n+1\rangle} - x_{\langle i+2\rangle,4}), \tag{19}$$

with the $\langle\ \rangle$ operator as introduced above, and the B^i_4 coefficient is given by

$$B^i_4 = -\sum_{n=1}^{3} B^i_n. \tag{20}$$

The effective diffusion coefficient is the $\Gamma_{\mathrm{eff},\phi}$ value at the centroid of the element, which can be calculated from the arithmetic mean of μ, k and ε at the nodes or by some other more convenient average procedure. It is assumed to prevail over the whole element.

The integration of the diffusive flux over the (plane) control sub-surface s is given by

$$\int_{S_s} \mathbf{J}^{\mathrm{D}}_\phi \cdot \mathbf{n} \, \mathrm{d}S = -\Gamma_{\mathrm{eff},\phi} S_s \left(\frac{\partial \phi}{\partial x_i}\mathbf{e}_i\right) \cdot \mathbf{n}_s = CD_{s,n}\phi_n \tag{21}$$

with the $CD_{s,n}$ coefficients given by

$$CD_{s,n} = -\frac{\Gamma_{\mathrm{eff},\phi} S_s}{\Delta}(B^i_n n_{s,i}), \tag{22}$$

where the summation convention does not apply to the s index. The discretization of the diffusive flux can lead to negative coefficients in the final discretization equation if highly distorted (non-Delaunay) elements are used.[16,23]

If ϕ is constant over one element, the ϕ partial derivatives are null over the element, and at a sub-control surface s, $\sum CD_{s,n} = 0$. Thus, each of the $CD_{s,n}$ coefficients can be expressed as the symmetric of the summation of the other three, that is,

$$CD_{s,k} = -\sum_{\substack{n=1 \\ n \neq k}}^{4} CD_{s,n}, \quad \forall k = 1, 2, 3, 4, \quad \forall s = 1, 2, 3. \tag{23}$$

4.3. *Integration of the convective flux I*

The integration of the convective flux over the (plane) control sub-surface s is given by

$$\int_{S_s} \mathbf{J}_{\phi}^{\mathrm{C}}.\mathbf{n}\, \mathrm{d}S = \int_{S_s} \rho \mathbf{V}\phi.\mathbf{n}\, \mathrm{d}S = \dot{m}_s \phi_{ip\,s}, \tag{24}$$

where $\phi_{ip\,s}$ is the value of ϕ at the integration point over the integration sub-surface s, and the mass flow rate $\dot{m}_s$ that crosses the s sub-surface is obtained from the expression

$$\dot{m}_s = \rho \langle \mathbf{V} \rangle_s . \mathbf{n}_s S_s. \tag{25}$$

The summation convention does not apply to (24) and (25). The term $\langle \mathbf{V} \rangle_s$ indicates an appropriate average over the sub-surface s. This will be discussed further later in the paper, in the context of mass flux interpolation. Within each element the centroidal value of ρ is assumed to prevail.

The problem is now to specify the sub-surface values $\phi_{ip\,s}$ in terms of the nodal values of ϕ. Special care is needed to do so because negative coefficients can arise in the final discretization equations. Here, the convective flux is integrated following the mass weighted scheme due to Schneider and Raw,[15] but adapted to the present elements and control sub-surfaces. Saabas[12] has called this adaptation the MAW (mass weighted) scheme.

4.4. *The mass-weighted scheme (MAW)*

The value of $\phi_{ip\,s}$ should be strongly dependent on the upstream value of ϕ with respect to the velocity $\langle \mathbf{V} \rangle_s$, and essentially independent of the downstream value of ϕ. This is accomplished through the mass weighted scheme of Schneider and Raw,[15] which is used here with the merits of physical realism in modelling the convective phenomenon and only positive contributions for the coefficients in the final discretization equations.

The MAW scheme is obtained by establishing the conservation principles of mass and Φ over each of the control sub-volumes contained in one elment, and considering the upstream character of the convection phenomenon when establishing the Φ conservation. Once this has been made to the four control sub-volumes in one element, each $\phi_{ip\,s}$ value is obtained as a function of the other $\phi_{ip\,s}$ values and also of the nodal values of ϕ. One obtain then[1,4,12,15,16]

$$\phi_{ip\,1} = f_1\phi_1 + (1 - f_1)[g_1\phi_{ip\,2} + (1 - g_1)\phi_2], \tag{26a}$$

$$\phi_{ip\,2} = f_2[g_2\phi_{ip\,1} + (1 - g_2)\phi_2] + (1 - f_2)[h_2\phi_{ip\,3} + (1 - h_2)\phi_4], \tag{26b}$$

$$\phi_{ip\,3} = (1 - f_3)\phi_3 + f_3[g_3\phi_{ip\,2} + (1 - g_3)\phi_4], \tag{26c}$$

where

$$f_1 = \max\left(\frac{|\dot{m}_1|}{\dot{m}_1}, 0\right), \quad g_1 = \max\left[\min\left(\frac{\dot{m}_2}{\dot{m}_1}, 1\right), 0\right], \tag{27a}$$

$$f_2 = \max\left(\frac{|\dot{m}_2|}{\dot{m}_2}, 0\right), \quad g_2 = \max\left[\min\left(\frac{\dot{m}_1}{\dot{m}_2}, 1\right), 0\right], \quad h_2 = \max\left[\min\left(\frac{\dot{m}_3}{\dot{m}_2}, 1\right), 0\right], \tag{27b}$$

$$f_3 = \max\left(\frac{|\dot{m}_3|}{\dot{m}_3}, 0\right), \quad g_3 = \max\left[\min\left(\frac{\dot{m}_2}{\dot{m}_3}, 1\right), 0\right], \tag{27c}$$

with the mass flow rates $\dot{m}_s$ defined in a direction similar to the outward unit normal $\mathbf{n}_s$, as in Figure 2. It should be noted that when $\dot{m}_s$ is zero, the product $\dot{m}_s\phi_{ips}$ (equation (24)) vanishes through $\dot{m}_s$ and the value of ϕ_{ips} is thus irrelevant.

The results of the MAW scheme (equation (26)) are written in the matrix form $[A]_{3\times3} \times [\phi_{ip}]_{3\times1} = [\mathrm{B}]_{3\times4}[\phi]_{4\times1}$, and in order to obtain the ϕ_{ips} values as functions of the nodal values ϕ_n only, we need to find the inverse matrix of the ϕ_{ips} coefficients on the left-hand side. The inversion process can be simplified due to the zero elements in the left-hand side. The inversion process can be simplified due to the zero elements in the left-hand side matrix, and the inverse matrix becomes

$$[A]^{-1} = \frac{1}{\Delta_{[A]}}\begin{bmatrix} 1-(1-f_2)h_2f_3g_3 & (1-f_1)g_1 & (1-f_1)g_1(1-f_2)h_2 \\ f_2g_2 & 1 & (1-f_2)h_2 \\ f_2g_2f_3g_3 & f_3g_3 & 1-(1-f_1)g_1f_2g_2 \end{bmatrix}, \tag{28}$$

where

$$\Delta_{[A]} = 1-(1-f_2)h_2f_3g_3-(1-f_1)g_1f_2g_2 \tag{29}$$

is the determinant of the left-hand side matrix. Multiplying now both sides of the obtained result of the MAW scheme by the inverse matrix $[A]^{-1}$ one obtains an equation that can be written formally as $[\phi_{ip}]_{3\times1} = [C]_{3\times4}[\phi]_{4\times1}$, which is the suitable form to express the ϕ_{ips} values at the control sub-surfaces as functions of the nodal values of ϕ. Another way is to refer one row at each time, which is the expression corresponding to the s control sub-surface (s can be 1, 2 or 3), to give

$$\phi_{ips} = [\mathrm{C}]_{s,n}\phi_n, \tag{30}$$

where the n index ranges from 1 to 4. As referred by Schneider,[4] the mass-weighted scheme presented is *almost* second-order accurate.

When ϕ is constant over one element, equation (30) gives, for each sub-control surface s, $\sum[C]_{s,n} = 1$. Thus each of the $[C]_{s,n}$ coefficients can be written as the difference to the unity of the summation of the other $[C]_{s,n}$, that is,

$$[C]_{s,k} = 1 - \sum_{\substack{n=1 \\ n\neq k}}^{4}[C]_{s,n}, \quad \forall k = 1,2,3,4, \quad \forall s = 1,2,3. \tag{31}$$

4.5. Integration of the convective flux II

ϕ_{ips} in (24) is replaced by the expression obtained with the MAW scheme (equation (30)), and the integration of the convective flux over the control sub-surface s becomes

$$\int_{S_s} \mathbf{J}_\phi^C.\mathbf{n}\, \mathrm{d}S = CC_{s,n}\phi_n, \tag{32}$$

with the $CC_{s,n}$ coefficients given by

$$CC_{s,n} = \dot{m}_s[C]_{s,n} \tag{33}$$

noting that the summation convention does not apply in (33).

Multiplying both sides of (31) by $\dot{m}_s$, and using the result of (33) one obtains

$$CC_{s,k} = \dot{m}_s - \sum_{\substack{n=1 \\ n \neq k}}^{4} CC_{s,n}, \quad \forall k = 1, 2, 3, 4, \quad \forall s = 1, 2, 3. \tag{34}$$

5. DISCRETIZATION EQUATION FOR ϕ

The discretization equation for ϕ is obtained by establishing the Φ conservation principle over each of the control volumes in the domain. This conservation principle is made through the assembling of the contributions of the control sub-volumes, which were derived above.

5.1. Discretization equation for an internal node

Each element gives its own contribution, through the control sub-volumes in which it is divided, to the establishment of the conservation equation for Φ in each of the control volumes that contain the nodes which are the vertices of the element under analysis. For the nodes in one element, retaining the way that the unit normal to each control sub-surface is directed (Figure 2), the control sub-surfaces that surround each control sub-volume, and using (23) and (34) in the more convenient way (the k index is chosen such that it coincides with the index of the node for which the conservation principle is being established), equation (10) becomes for each interior node P of the domain

$$\left[\sum_{nb} a_{nb} - \sum_{nc} V_{nc}(S_{\phi,P})_{nc}\right]\phi_P = \sum_{nb} a_{nb}\phi_{nb} + \sum_{nc} V_{nc}(S_{\phi,C})_{nc}, \tag{35}$$

where the summation convention does not apply. The summation in nb is made over the neighbouring nodes of node P, and the summation in nc is made over the control sub-volumes that, when assembled, form the entire control volume associated with node P.

The last summation on the right-hand side of (35) can be written as

$$\sum_{nc} V_{nc}(S_{\phi,C})_{nc} = V_P\langle S_{\phi,C}\rangle_P, \tag{36}$$

where

$$V_P = \sum_{nc} V_{nc} \tag{37}$$

is the volume of the control volume associated with node P, and

$$\langle S_{\phi,C}\rangle_P = \frac{1}{V_P}\sum_{nc}(S_{\phi,C})_{nc}V_{nc} \tag{38}$$

is the mean value of $S_{\phi,C}$ in the control volume. Submitting the second summation on the left-hand side of (35) to a similar treatment, (35) reads

$$a_P\phi_P = \sum_{nb} a_{nb}\phi_{nb} + bb_p, \tag{39}$$

where

$$a_P = \sum_{nb} a_{nb} - V_P\langle S_{\phi,P}\rangle_P \tag{40}$$

and

$$bb_P = V_P \langle S_{\phi,C} \rangle_P. \tag{41}$$

All contributions of the discretized convective transport terms to the coefficients a_{nb} in (39) are positive (this is ensured by the MAW scheme). Furthermore, Delaunay elements are recommended to ensure that the discretized diffusive transport terms also contributes positively to a_{nb}.[16,23] Owing to the fact that $S_{\phi,P} \leqslant 0$ (equation (15)) the a_P coefficient is obtained as a sum of positive terms only, and $|a_P| \geq |a_{nb}|$. This *dominance of the central coefficient* is of major importance to find the iterative type of solution for the resulting system of algegraic equations. Finally, the a_{nb} coefficients are the same for the three velocity components, their discretization equations differing only by the a_P and bb_P coefficients.

5.2. *Discretization equation for a boundary node*

As stated in the integral conservation equation (equation (10)), the portion of the control surface that is coincident with the domain boundary should also be travelled in the integration process, in order to close the control surface. This is made through an additional integral extended over the control surface that coincides with the physical boundary. From (10) and (35), it can be stated that the conservation equation for a boundary node is similar to (39) but with

$$bb_P = V_P \langle S_{\phi,C} \rangle_P - (\dot{F}_B + \dot{m}_B \phi_P), \tag{42}$$

where $\dot{m}_B$ and $\dot{F}_B$ are, respectively, the mass flow rate and the total (convective plus diffusive) rate of Φ leaving the domain through the boundary that coincides with the control surface associated with the node P.

5.3. *Boundary conditions for* ϕ

There are essentially three types of boundary conditions: no-flow, inflow, and outflow.

A no-flow boundary means that an impermeable wall coincides with the boundary location and $\dot{m}_B = 0$. At such a boundary, either the value of the dependent variable ϕ is specified or a relationship about the flux at the boundary $\dot{F}_B$ is known.

At an inflow boundary, the value of ϕ must be specified, and is usually known. This information is introduced in the discretization equation through the manipulation of the a_P and bb_P coefficients. To do so, we make $a_P = G$ and $bb_P = G\phi_{\text{specified}}$ where G is a great number, usually $G = 10^{30}$. The a_P and bb_P coefficients are dominant in the discretization equation which reduces to $\phi_P = \phi_{\text{specified}}$. This practice is advantageous by the following reasons. First, one need change only two coefficients and not all the neighbouring coefficients (26 in this case). Second, the coefficients in the discretization equations for the velocity components are the same, exception made to the a_P and bb_P. Thus, we only need to have one discretization equation for all the velocity components with the possibility of changing the values of a_P and bb_P.

At an outflow boundary, neither the value nor the flux of ϕ are known. This apparent difficulty is solved by noting that at the outflow boundaries the diffusive influences are negligible as compared with the convective ones, and we can make $\dot{F}_B \approx m_B \phi_B$, where ϕ_B is some suitable average value of ϕ at the boundary. An interesting practice is obtained with $\phi_B = \phi_P$, no additional information being needed at the outflow boundary as given by (42). In other words, (39), obtained for an internal node, applies also for an outflow boundary node.

6. FLOW FIELD CALCULATION

The major problem to solve now is: how to obtain an equation for the pressure from the continuity equation that does not contain the pressure explicitly? We follow the essentials of the method proposed by Prakash and Patankar[9] for two-dimensional situations. This procedure has been successfully used by Costa *et al.*[1,2] for two-dimensional CVFEMs and by Saabas and Baliga[17,18] for two and three-dimensional CVFEMs, by Rice and Schnipke[24] for two-dimensional FEMs, and by Peric *et al.*[25] for two-dimensional FVMs.

6.1. Discretization equations for the velocity components

The analogue of (41) becomes, for the u_i velocity component,

$$bb_P^{u_i} = V_P \langle S_{u_i,C} \rangle_P = V_P \left\langle S_C^{u_i} - \frac{\partial p}{\partial x_i} \right\rangle_P . \tag{43}$$

If the part of the bb_P term which is independent of the pressure is designated by b_P, the discretization equation for the u_i velocity component becomes, in the form of (39),

$$a_P^{u_i} u_{i_P} = \sum_{nb} a_{nb} u_{i_{nb}} + b_P^{u_i} - V_P \left\langle \frac{\partial p}{\partial x_i} \right\rangle_P \tag{44}$$

or

$$u_{i_P} = \hat{u}_{i_P} - d_P^{u_i} \left\langle \frac{\partial p}{\partial x_i} \right\rangle_P , \tag{45}$$

where the pseudo-velocity $\hat{u}_{i_P}$ is defined as

$$\hat{u}_{i_P} = \frac{\sum_{nb} a_{nb} u_{i_{nb}} + b_P^{u_i}}{a_P^{u_i}} \tag{46}$$

and the pressure coefficient $d_P^{u_i}$ is given by

$$d_P^{u_i} = V_P / a_P^{u_i} . \tag{47}$$

At this point it should be noted that (45) states that the velocity components, as given by the momentum equations, can be expressed as a sum of two terms: the explicit pressure influence, and the remaining influences that contain no pressure. This is an important aspect because one of the problems to solve in this section is to introduce explicitly the pressure into the continuity equation through the velocities contained in it. When the velocity is specified at a node, if the corresponding value is introduced as a boundary condition through the manipulation of a_P and bb_P as given above, the a_P coefficient is comparatively great and the pressure coefficient vanishes to zero, thus making this velocity independent of the pressure and the nodal pseudo-velocity equal to the nodal velocity, as desired.

6.2. The mass conserving velocity field

For the integration of the continuity equation, the mass flux $\mathbf{J}^m$ is, in principle, derived using the velocity field $\mathbf{V} = u_i \mathbf{e}_i$. This way is obvious, but there are serious problems associated with this practice.

First, if such a mass flux were used in (10) (with zero source and diffusion terms and $\phi = 1$) the result would be an equation in terms of the nodal velocities $(u_i)_n$ and not in terms of nodal pressures, as desired. Second, if (45) were used to substitute the nodal velocities $(u_i)_n$ in the so obtained equation,

such an equation should account explicitly for the pressure and, in principle, a discretization equation for this variable could be obtained. However, the resulting equation, in the form of (39), can unfortunately contain only non-neighbouring nodes of the node P, which is a singularity for the obtained system of equations. In conclusion, a more suitable mass conserving velocity field needs to be found to compute the mass flux entering in (10).

Taking guidance from (45), within each element, a mass conserving velocity field defined by

$$u_i^m = \hat{u}_i - d^{u_i}\left(\frac{\partial p}{\partial x_i}\right)_e \tag{48}$$

could be used to obtain a suitable discretization equation for the pressure. The nodal values of the pseudo-velocities are given by (46), the nodal values of the pressure coefficients are given by (47), and all these quantities are assumed to vary linearly with the x_i co-ordinates within each element. The subscript e is used to mean that $\partial p/\partial x_i$ corresponds to one element, and as the pressure is assumed to vary linearly within each element (this assumption is consistent with the elliptic character of the pressure), these pressure gradient components are constant in each element.

At this point, it should be noted that as the velocity field given by (48) verifies mass conservation, the mass flow rates used in the integration of the convective flux by the MAW scheme should be calculated using this same mass conserving velocity field. The use of two different velocity fields can be seen as an inconsistency of the method, but it is the price to pay when using control volume equal-order finite element methods, or non-staggered finite difference methods for fluid flow calculations.[1,9,12,24,25]

6.3. Integration of the continuity equation

The mass flux based on the mass conserving velocity field given by (48) is integrated assuming (as for the integration of the convective fluxes) that, within an element, the centroidal value of density prevails, and the pseudo-velocities and pressure coefficients vary linearly. Thus, in a element,

$$u_i^m = \hat{u}_i - d^{u_i}\left(\frac{\partial p}{\partial x_i}\right)_e = \hat{u}_i - \frac{d^{u_i}}{\Delta} B_n^i p_n, \tag{49}$$

where the summation convention does not apply to the i index.

The integration of the mass flux over the (plane) control sub-surface s is made in a way similar to that of the convective flux to give

$$\int_{S_s} \mathbf{J}^m.\mathbf{n}\, \mathrm{d}S = CP_{s,n} p_n + BP_s, \tag{50}$$

with

$$CP_{s,n} = -\frac{\rho_s S_s}{\Delta} d_s^{u_i} B_n^i n_{s,i} \tag{51}$$

and

$$BP_s = \rho_s S_s \hat{u}_{i,s} n_{s,i}, \tag{52}$$

where the summation convention does not apply to the s index and to the $d_s^{u_i} B_n^i$ product.

One should note the similarity between the $CD_{s,n}$ coefficients given by (22) and the $CP_{s,n}$ coefficients given by (51), and the result given by (23) is also valid for the $CP_{s,n}$ coefficients. As it was noticed when integrating the diffusive flux, with Delaunay elements, it contributes only with positive

coefficients for the final discretization equation, and the same is valid for the pressure discretization equation.

6.4. *Discretization equation for p at an internal node*

Following a way similar to that used to obtain the discretized equation for ϕ, we obtain, at each node, a pressure discretization equation that establishes mass conservation over the control volume associated with the internal node P. This can be written, in the form of (39), with $a_P^p = \sum a_{nb}^p$,

$$a_P^p p_P = \sum_{nb} a_{nb}^p p_{nb} + bb_P^p, \tag{53}$$

with the nb summation extended to the neighbouring nodes of node P, and the summation convention does not apply.

6.5. *Discretization equation for p at a boundary node*

Following the arguments invoked when establishing the ϕ discretization equation at a boundary node, the discretization equation for p at a boundary node can be obtained as

$$a_P^p p_P = \sum_{nb} a_{nb}^p p_{nb} + bb_P^p - \dot{m}_B, \tag{54}$$

where $\dot{m}_B$ is the mass flow rate leaving the domain through the boundary associated with the node P.

6.6. *Boundary conditions for p*

There are essentially two types of boundary conditions for the p equation: known pressure, or specified mass flow rate.

If the pressure is specified at the boundary node, (54) is reduced to $p_p = p_{\text{specified}}$.

If the mass flow rate is specified, $\dot{m}_B$ is easily evaluated and incorporated in (54).

6.7. *Treatment of the boundary conditions introduced by the wall law*

For the general velocity parallel to a wall, $\mathbf{V}_{||}$, the fixed wall influence is always a loss of momentum so that τ_w and $\mathbf{V}_{||}$ have opposite signs. Then, (2) can be written, in terms of forces as $\mathbf{F}_w = -(\lambda_w A_w)\mathbf{V}_{||}$, where A_w is the area over which τ_w acts. We note that $\mathbf{V}_{||}$ is the velocity component parallel to the wall which, in the general case, has three non-zero components, and for the co-ordinate direction i the relation is $F_{w,i} = -(\lambda_w A_w)V_{||,i}$.

The surface unit outward normal $\mathbf{n}$ is easily known from the co-ordinates of the nodes of the triangular two-dimensional element which is the face of the tetrahedral element that coincides with the domain boundary. The velocity component perpendicular to the surface is calculated as $\mathbf{V}_\perp = M_\perp \mathbf{n}$ with $M_\perp = u_i n_i$. The parallel component, $\mathbf{V}_{||}$, can now be easily evaluated as $\mathbf{V}_{||} = \mathbf{V} - \mathbf{V}_\perp$, and the components of $\mathbf{V}_{||}$ are $V_{||,i} = u_i - M_\perp n_i$. Introducing the expressions for $\mathbf{V}_{||,i}$ and $M_\perp$ in the expression of $F_{w,i}$ we obtain, for the force components,

$$F_{w,i} = -(\lambda_w A_w)\left[u_i(1 - n_i^2) - \sum_{\substack{j=1 \\ j\neq i}}^{3} u_j n_i n_j\right], \tag{55}$$

where the summation convention does not apply.

The treatment of the boundary conditions due to the use of the wall law in the momentum equations are given in an integrated form by (55). Noting the particular form of (55), for the u_i velocity component, the symmetric of the term $-(\lambda_w A_w)(1 - n_i^2)$ that multiplies u_i, which is always positive, is introduced in the $a_P^{u_i}$ coefficient, the remaining terms being introduced in the $bb_P^{u_i}$ coefficient.

7. PROCEDURE CLOSURE

7.1. Under-relaxation, solution, convergence and pressure level

Under-relaxation. With the procedure proposed by Patankar,[14] from (39) the following equation is obtained

$$\frac{a_P}{\alpha}\phi_P = \sum_{nb} a_{nb}\phi_{nb} + bb_P + (1-\alpha)\frac{a_P}{\alpha}\phi_P{}^*, \tag{56}$$

where α is the *under-relaxation factor*. The under-relaxation, which is introduced before the resolution of the equations, is made only by changing the a_P and bb_P coefficients as it is evident from (56). In the test problems, a value of $\alpha = 0{\cdot}5$ for all the variables other than p was found to give good results. In the proposed method, the pressure equation is not under-relaxed, and the pseudo-velocities and pressure coefficients are evaluated before the under-relaxation operation is performed. There are two reasons for this procedure: (i) if we under-relax the pressure equation the mass conservation principle is degraded; and (ii) Majumdar[26] has shown (in the context of finite differences) that the under-relaxation must be carefully performed when using non-staggered grids with control volume finite difference methods, because the final solution can depend on the under-relaxation factor; the problem is the same when using equal–order control volume finite element methods. To avoid this dependence, either one stores the velocity components in each control sub-surface in a element, or one performs the under-relaxation after evaluation of the pseudo-velocities and pressure coefficients. The latter way is preferred due to its simplicity and no additional needs of storage capacity.

Solution. For each particular ϕ and for p, and at each iteration level, there is a system of N_n algebraic equations like (39) that needs to be solved, where N_n is the number of nodes in the domain. As the equations for ϕ are similar to that for p, the same solver can be used to solve all these equations. Iterative methods are viable and practical for the solution of the proposed discretization equations system, because the positivity of the coefficients and the diagonal dominance of such systems guarantee the convergence of the iterative methods. To accelerate the convergence we use a line Gauss–Seidel method, in which we solve for each line in the domain with the TDMA algorithm.[14] When the coefficients in the discretization equations become strongly anisotropic, the TDMA solver can stall, and we use a block-correction 2D and 1D procedure added to the solver.[27] This was found to be especially important when solving the pressure discretization equations.

Convergence. A suitable stop criterium is to test whether the summation of the equations residuals is sufficiently small in the domain for each particular ϕ and for p. Thus, it is tested whether the relation

$$\left[\sum \left| a_P\phi_P - \sum_{nb} a_{nb}\phi_{nb} - bb_P \right| \right] \Big/ \left[\sum |(\dot{F}_B)_{\text{in}}|\right] < \delta_\phi, \tag{57}$$

where the summation is made over all the nodes other than those where ϕ has a specified value and the subscript in refer the inlet boundaries, is satisfied for any suitable small value of δ_ϕ. Owing to the iterative nature of the method, the discretization equations contain only tentative coefficients, and it is thus a bad practice to spend an excessive amount of work to verify the relation (57) with very small values of δ_ϕ. Only the pressure equation (mass conservation equation) must be solved to satisfy relation (57) with a small value of δ_p because all the method is based in a flow field for which the mass conservation is verified.

Pressure level. In incompressible flow calculations the pressure level is irrelevant, and only the pressure differences are considered in the Navier–Stokes equations. In order to maintain the pressure

level within acceptable values and small round-off errors, it is a good practice to refer the pressure to that of a point in the domain for which the pressure is made to be zero.

7.2. *Summary of the method for implementation*

For implementation purposes one now summarize the method described above. Once the grid has been defined, the following major steps must be performed.

1. Velocity field, pressure field, and other scalar fields are guessed.
2. The properties are calculated and stored at each node. The mass flow rates at the outflow boundaries are calculated, and they are affected by a correction factor in order to guarantee that the global mass conservation is satisfied in the domain. Once convergence is obtained this multiplicative factor will be one, and does not affect the final solution.
3. The a_{nb} discretization coefficients for the velocity components, the same for all of them, are calculated.
4. The source terms, without pressure, are integrated for the u_i equations, and the result introduced in the $a_P^{u_i}$ and $b_P^{u_i}$ coefficients. The additional integrated terms due to the boundary conditions imposed over the momentum equations by the wall law are also calculated and introduced in the $a_P^{u_i}$ and $b_P^{u_i}$ coefficients.
5. The additional boundary conditions for the u_i equations are introduced by manipulation of the $a_P^{u_i}$ and $b_P^{u_i}$ coefficients.
6. The pseudo-velocities and pressure coefficients are calculated.
7. The discretization equations for pressure are obtained, boundary conditions are introduced, and the system of equations is solved to obtain the new values of p.
8. The integration of the pressure gradient components is performed over each control volume and added to the $b_P^{u_i}$ coefficients.
9. The under-relaxation of the u_i equations is made and the new values for u_i are obtained, one at each time.
10. For the other scalar dependent variables that are coupled with the flow field, one at each time, the coefficients a_{nb} are calculated, and the integration of the source term is performed. Boundary conditions are introduced, equations are under-relaxed, and finally the so obtained discretization equations are solved to find the new ϕ field.
11. At this point suitable convergence tests are performed. If the convergence tests are not satisfied, the procedure should be returned to step 2. Otherwise, the procedure goes ont to step 12.
12. The procedure described in 10 is applied to the remaining ϕ variables that have no influence over the flow field. The equations for these variables must be solved in some considerable extent, as their calculated values are the final solution.

7.3. *Concluding remarks*

The coefficients a_{nb} in the pressure equations are obtained from the pressure coefficients d^{u_i}, which are assumed to vary linearly within each element. If an element is placed in the domain in such a way that all the four nodes are in the boundary, with imposed velocities, the pressure coefficients are zero within the element. If the contributions to the a_{nb} coefficients in the pressure equation for one of these nodes are obtained only from such a boundary element, a zero a_P coefficient to the equation will result, and the pressure cannot be calculated at this node. This is a bad equation for the pressure, and the domain must be discretized in such a way that there are no elements with all the vertices at specified-velocity boundaries.

In the integration of the diffusive fluxes it is assumed that ϕ varies linearly with the x_i co-ordinates within each element, while the integration of the convective fluxes is made from a qualitative/quantitative analysis of the convective phenomenon. Such a procedure seems to be inconsistent, but leads to an overall method that results. Some more consistent alternatives were designed,[10,11] but it was found that additional sophistication and consistence are companions of additional problems.

The mass conserving velocity field used here is defined somewhat *ad hoc* but leads to a good discretization equation for the pressure; however, this is a common characteristic of the control volume based equal-order finite element methods and non-staggered finite difference methods. Prakash[10] and Hookey[11] have constructed some more consistent mass conserving velocity fields, but the resulting procedure suffers from problems that can limit the situations where it can be applied, and some of them can even cause the overall procedure to fail.

8. APPLICATIONS

Validation of the method presented above is now performed through its application to two different test problems, followed by comparison with available experimental and also numerical results, obtained with the well established finite difference method. All the test problems analysed correspond to high Reynolds numbers in order to legitimate the application of the k-ε turbulence model that was used in the present formulation.

8.1. Three-dimensional deflected turbulent jet

Problem statement. When a jet is deflected by a stream normal to its axis a three-dimensional flow results. A qualitative representation of this flow field, taken from the work of Patankar *et al.*[28], is sketched in Figure 3. The bending of the jet, the perturbations introduced in the main stream, and a secondary motion in the form of two vortices in the cross section of the deflected jet are some of the most important characteristics of such a flow. As the fluid (of constant density) is the same in the main stream and in the jet, one of the most important parameters is R, the ratio of the injection velocity to the main stream velocity.

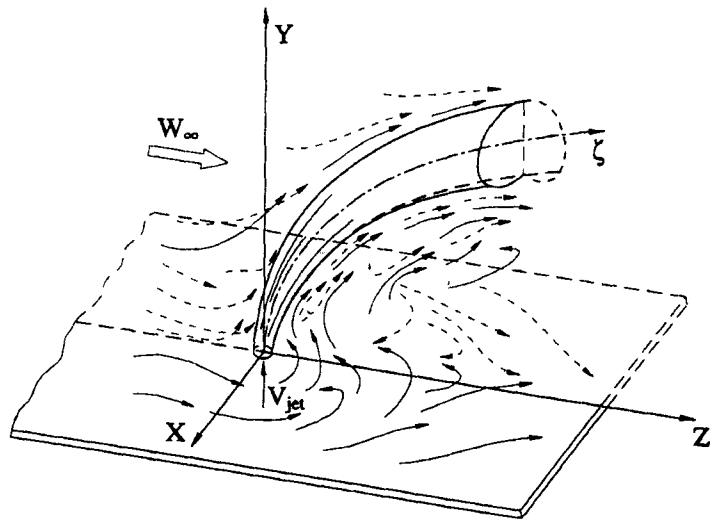

Figure 3. Schematic representation of three-dimensional deflected turbulent jet flow[28]

Computational details. Following Patankar *et al.*[28] and Saabas,[12] the problem is solved in the dimensional form within a box-shaped domain, and the symmetry of the flow about the yz plane is considered. In the x direction the domain extends from the symmetry plane ($x=0$) to $x_i=10r_0$, r_0 being the radius of the injection hole. In the y direction, the domain begins at the wall, and its upper surface is placed sufficiently far way to guarantee uniform main stream conditions there; depending on the particular R considered, exploratory calculations are needed to define the upper surface location. We used $y_t=16r_0$ for $R=2{\cdot}37$, $y_t=18r_0$ for $R=3{\cdot}95$ and $y_t=22r_0$ for $R=6{\cdot}35$. In the z direction, the upstream surface is placed at $z=-4r_0$, and the downstream surface is placed at such a distance that the mean jet velocity there became nearly parallel to the z-direction. We used $z=18r_0$ for the location of this surface, the total length in this direction being thus $z_t=22r_0$. The $11\times19\times19$ grid used here is expanded along the three directions, and the expansion factor is defined in such a way that the (circular) injection hole can be modelled as a rectangle (with 2×3 nodes) with the same area. The boundary conditions for the velocity field were specified as: (i) at $x=0$ (symmetry plane) $u=0$, together with zero gradients of all other velocities and pressure; (ii) at $x=x_t$, $y=y_t$ and $z=-4r_0$, we have $u=v=0$, and $w=W_\infty$ (exception made to the points at the wall, where $w=0$); (iii) at the injection hole $u=w=0$, $v=V_{\text{jet}}$, and for calculation of the mass entering it is assumed that V_{jet} prevails over the whole hole; and (iv) for the points in the first grid plane next to the wall the boundary conditions imposed by the wall law are considered. The following values were adopted: $r_0=0{\cdot}02$m, $R=2{\cdot}37$ with $V_{\text{jet}}=8{\cdot}17$m/s, $R=3{\cdot}95$ with $V_{\text{jet}}=16{\cdot}95$m/s, and $R=6{\cdot}35$ with $V_{\text{jet}}=20{\cdot}7$m/s, which give jet Reynolds numbers of 21,200, 41,500 and 53,600 respectively. For the turbulence variables k and ε the boundary conditions were specified as: (i) zero gradients of k and ε at $x=0$; (ii) at $x=x_t$, $y=y_t$ and $z=-4r_0$ the turbulence kinetic energy is that of the free stream with a turbulence intensity of $0{\cdot}01$, and ε is given by the corresponding inflow equation with $l=0{\cdot}05y_t$; (iii) at the injection hole k and ε are given by their inflow equations, with a turbulence intensity of $0{\cdot}025$, and $l=2r_0$; and (iv) for the points in the first grid plane from the wall k and ε are given by (4) and (5), respectively. Convergence is obtained after 200 overall iterations with $\delta_\phi=5\times10^{-5}$ for the u_i components, $\delta_p=2\times10^{-5}$ for the pressure, and $\delta_\phi=10^{-5}$ for k and ε. The required CPU time is of 45 s per global iteration on a VAX 9210 computer.

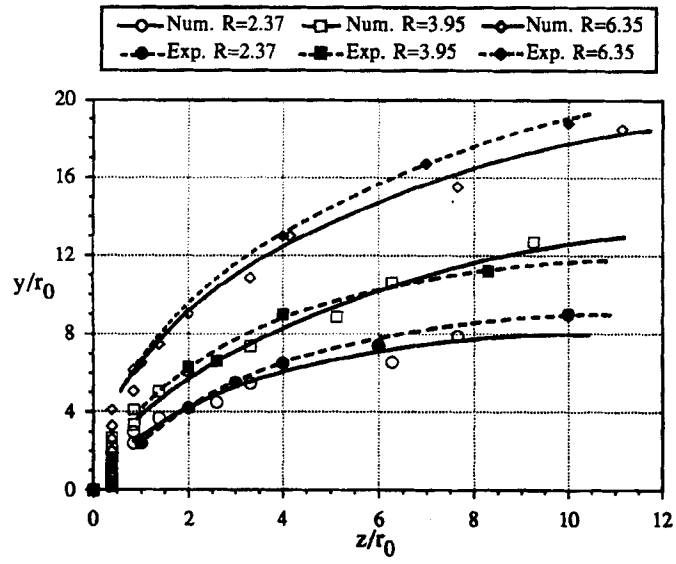

Figure 4. Locus of maximum velocity on the symmetry plane (experimental data from Reference 29)

Results. The calculated results include the locatin of the jet centreline, defined as the locus of maximum velocity on the symmetry plane. The results for the centreline of the jet in Figure 4 agree very well with the numerical ones of Patankar *et al.*,[28] obtained in a 10 × 15 × 15 grid, and also with the experimental ones of Chassing *et al.*[29] Plots of the computed velocity field exhibits all the characteristics of the expected flow as schematically represented in Figure 3. Saabas[12,18] has also analysed this problem with similar encouraging conclusions.

8.2. Flows in 90° and 45° junctions of ducts with rectangular cross sections

Problem statement. The study of flow in junction ducts represented in Figure 5 is important for the knowledge of the influences of each flow over the other, thus determining the characteristics of the resulting joining flow. As the cross sections of the ducts are rectangular, a secondary flow due to the boundary layer interaction will be expected. One of the most important parameters is R, the ratio of the mass flow rate in one of the entry ducts to the total exit mass flow rate of the joined flows.

Computational details. The problem is solved in its dimensional form in the domain of Figure 5 for the 90° junction, and in one that results from it by a 45° rotation of branch 2 about the line PP'. The discretization grids are 7 × 13 × 41 for branch 1 and 7 × 13 × 17 for branch 2, both with some contraction in the regions of expected intense gradients. In the interest of saving the storage capacity required, the discretization equations are obtained separately for each branch, and a special form of the solver was designed to implicitly solve for the whole domain. Additionally, symmetry about the yz plane is considered. Boundary conditions for the velocity field were specified as: (i) at the walls of both branches $u = v = w = 0$; (ii) at the symmetry plane $x = 0$, $u = 0$ and zero gradients for all other velocity components and pressure; (iii) for the points in the first grid planes from the walls the boundary conditions imposed by the wall law were considered; (iv) at the inlets of both branches the existence of boundary layers was considered, the velocity profile being obtained from the logarithmic law with the wall shear stress extracted from the friction coefficient given by Blasius formula (the logarithmic profile is used only when it gives a velocity less than the bulk velocity); and (v) the inlet velocities are perpendicular to the domain boundary at the inlet sections. The mass flux ratio R, which for incompressible flows is also a velocity ratio, is $R = 0{\cdot}75$ for both 90° and 45° junctions and is based on the mass flux entry of branch 2. for the 90° junction, the exit bulk velocity is $W_{ref} = 41{\cdot}8$m/s with a corresponding Reynolds number of 91,692, and for the 45° junction, the exit bulk velocity is $W_{ref} = 39{\cdot}6$m/s with a corresponding Reynolds number of 86,866, the Reynolds number being based

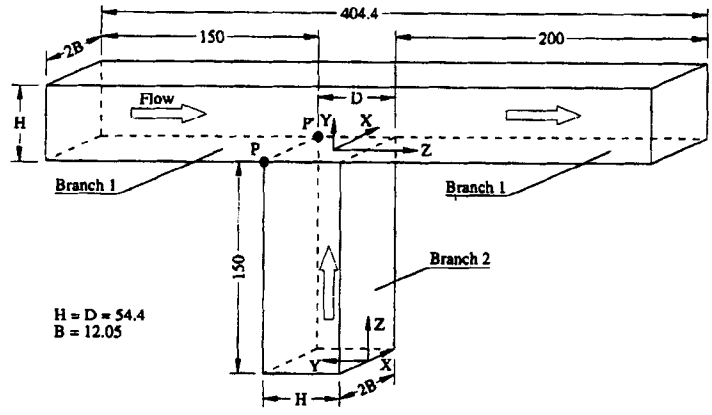

Figure 5. Domain for the junction flow calculation (dimensions in mm)[30]

on the hydraulic diameter which is equal in both ducts. For the turbulence variables k and ε the boundary conditions were specified as: (i) at $x=0$ the gradients of both k and ε are zero; (ii) for the points in the first grid planes from the walls k and ε are given by (4) and (5) respectively; and (iii) at the inlet planes, exception made to the points adjacent to the walls, k and ε are given by the equations for k and ε at the inflows, with a turbulence intensity of 0·03 and $l=0{\cdot}15D_h$, D_h being the hydraulic diameter equal for both branches. Convergence is obtained after 250 overall iterations with $\delta_\phi = 5 \times 10^{-5}$ for the u_i components, $\delta_p = 10^{-4}$ for the pressure, and $\delta_\phi = 10^{-4}$ for k and ε. The required CPU time is of 48 s per global iteration on a VAX 9210 computer.

Results. Results are presented for the v and w velocities at some interesting planes in the domain, over the yz symmetry plane, for the 90° junction in Figure 6 and for the 45° junction in Figure 7. The

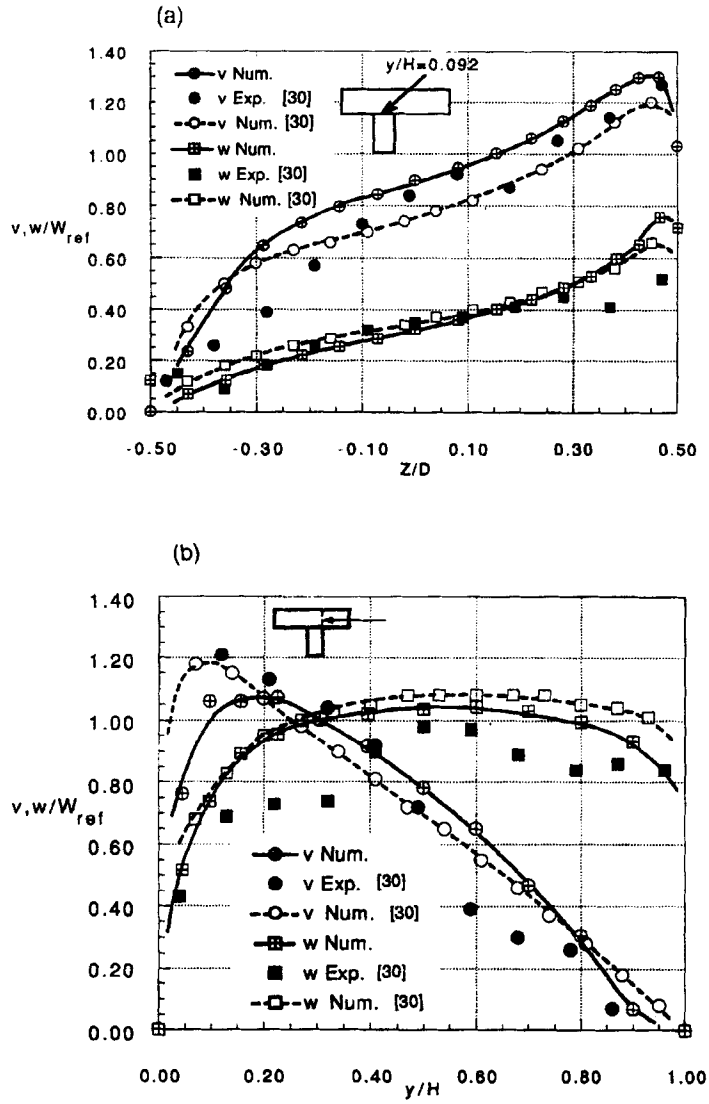

Figure 6. Velocities u and v at some interesting planes for the 90° junction

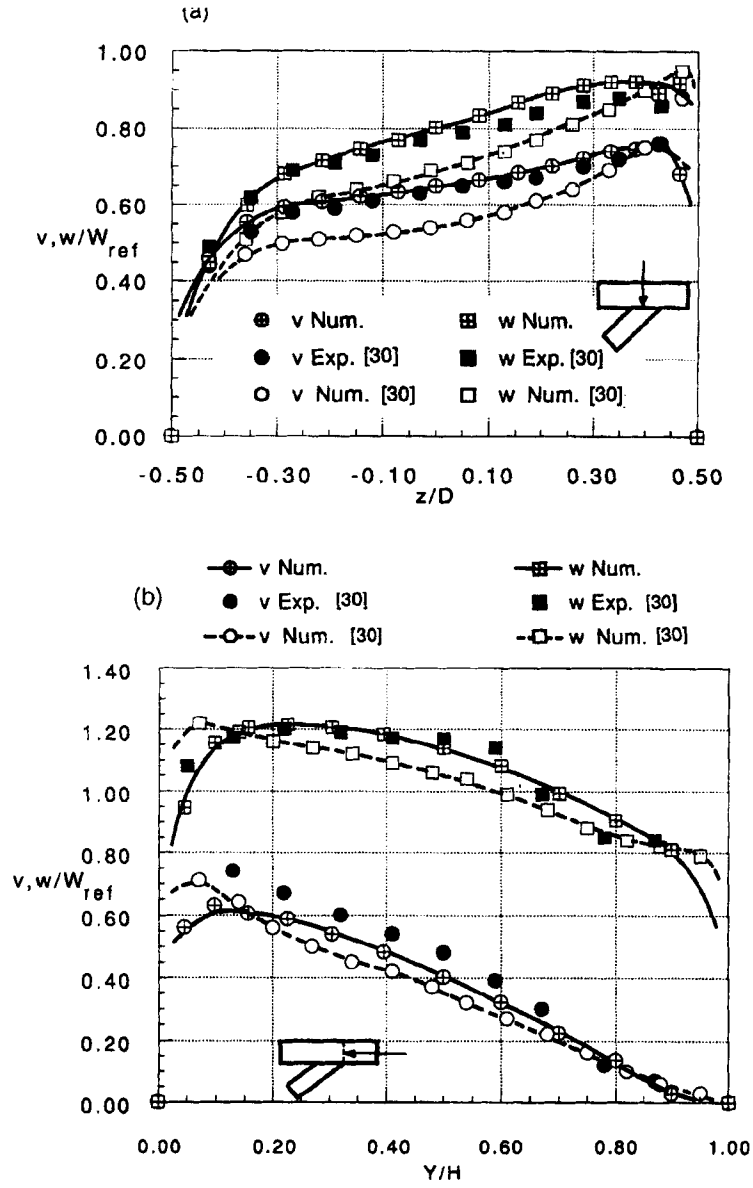

Figure 7. Velocities u and v at some interesting planes for the 45° junction

present velocity predictions agree satisfactorily well with the numerical and experimental ones of Dimitriadis,[30] the latter having been obtained on a $8 \times 18 \times 55$ grid for the 90° junction and on a $12 \times 30 \times 80$ grids for the 45° junction. Plots of the computed velocity fields present also all the characteristics that were detected experimentally and numerically by Dimitriadis.[30]

9. CONCLUSIONS

In this paper, the formulatin and some examples of application of an equal-order CVFEM for three-dimensional incompressible turbulent fluid flow, heat trasfer, and related phenomena have been

presented and tested. The flexibility of handling complex geometries without additional difficulties in the essentials of the method are some of its most attractive features. Comparison of the reuslts obtained with fully independent experimental and numerical ones are very encouraging regarding the capabilities of the method. Also a qualitative analysis of the calculated flow field shows that the present methodology is capable of capturing the main features of the flows considered. The required number of iterations is relatively small, but the CPU time required for one iteration is greater than that in finite-difference methodology. As far as we know, there are no formal limitations for the scheme. The method is presented together with a structured mesh, but this is only due to reasons of implementation convenience; the essential aspects are derived on an element-by-element basis and are not affected by the overall mesh used. The only problem that can arise with the used mesh is a discretization equation for the pressure with zero coefficient a_P, as referred in Section 7.3. However, this only affects a particular type of corner element, whose use can be easily avoided.

ACKNOWLEDGEMENTS

The authors acknowledge the contribution of Professor Rabi Baliga (McGill University, Montreal, Canada), who made many interesting suggestions on the first draft of this paper.

REFERENCES

1. V. A. F. Costa and L. A. Oliveira, 'A control volume based finite element method for two-dimensional steady fluid flow, heat transfer, and related phenomena', In *Proc. III Encontro de Mecânica Computacional*, vol. 2, pp. F10.1–F10.15, Coimbra, Portugal, 1992.
2. V. A. F. Costa, A. R. Figueiredo, and L. A. Oliveira, 'Convecção natural em cavidades paralelogrâmicas', in *Proc. I Congreso Iberoamericano de Ingeniería Mecánica*, vol. 2, pp. 255–260. Madrid, Spain, 1993.
3. A. J. Baker, *Finite Element Computational Fluid Mechanics*, McGraw-Hill/Hemisphere, New York, 1983.
4. G. E. Schneider, 'Elliptic systems: finite-element method I', in Minkowycz, W. J., Sparrow, E. M., Schneider, G. E., and Pletcher, R. H. (ed.), *Handbook of Numerical Heat Transfer*, Ch. 10, pp. 379–420, Wiley, New York, 1988.
5. B. R. Baliga, A control-volume based finite element method for convective heat and mass transfer, Ph. D. Thesis, Dept. of Mech. Eng., University of Minnesota, MN, 1978.
6. B. R. Baliga and S. V. Patankar, 'A new finite-element formulation for convection-diffusion problems', *Numer. Heat Transfer*, **3**, 393–409 (1980).
7. B. R. Baliga and S. V. Patankar, 'A control volume finite-element method for two-dimensioinal fluid flow and heat transfer', *Numer. Heat Transfer*, **6**, 245–261 (1983).
8. B. R. Baliga and S. V. Patankar, 'Elliptic systems: finite-element method II', in Minkowycz, W. J. Sparrow, E. M., Schneider, G. E., and Pletcher, R. H. (eds.), *Handbook of Numerical Heat Transfer*, Ch. 11, pp. 421–461, Wiley, New York, 1988.
9. C. Prakash, and S. V. Patankar, 'A control volume-based finite-element method for solving the Navier-Stokes equations using equal-order velocity-pressure interpolation', *Numer. Heat Transfer*, **8**, 259–280 (1985).
10. C. Prakash, 'An improved control volume finite element method for heat and mass transfer, and for fluid flow using equal-order velocity-pressure interpolation', *Numer. Heat Transfer*, **9**, 253–276 (1986).
11. N. A. Hookey, Evaluation and enhancements of control volume finite element methods for two-dimensional fluid flow and heat transfer, M. Eng. Thesis, Dept. of Mech. Eng., McGill University, Montreal, 1986.
12. H. J. Saabas, A control volume finite element method for three-dimensional, incompressible, viscous fluid flow, Ph. D. Thesis, Dept. of Mech. Eng., McGill University, Montreal, 1991.
13. B. R. Baliga and H. J. Saabas, 'Control volume finite element methods for incompressible fluid flow', in *Proc. III Encontro de Mecânica Computacional*, Keynote Lecture on Fluid Dynamics, vol. 1, pp. C2.1-C2.20, Coimbra, Portugal, 1992.
14. S. V. Patankar, *Numerical Heat Transfer and Fluid Flow*, Hemisphere/McGraw-Hill, Washington, DC, 1980.
15. G. E. Schneider and M. J. Raw, 'A skewed positive influence coefficient upwinding procedure for control-volume-based finite element convection diffusion computation', *Numer. Heat Transfer*,. **9**, 1–26 (1986).
16. C. Masson, H. J. Saabas, and B. R. Baliga, 'Co-located equal order control-volume finite element method for two-dimensional axisymmetric incompressible flow', *Int. J. Numer. Methods Fluids*, **18**, 1–26 (1994).
17. H. J. Saabas and B. R. Baliga, 'A co-located equal-order control-volume finite element method for multi-dimensional, incompressible, fluid flow—Part I: Formulation', *Numer. Heat Transfer*: Part B—Fundamentals (to be published).
18. H. J. Saabas and B. R. Baliga, 'A co-located equal-order control-volume finite element method for multi-dimensional, incompressible, fluid flow—Part II: Verification', *Numer. Heat Transfer*: Part B—Fundamentals (to be published).
19. B. E. Launder and D. B. Spalding, *Mathematical Models of Turbulence*, Academic Press, London, 1972.
20. B. E. Launder and D. B. Spalding, 'The numerical computation of turbulent flows', *Comp. methods appl. mech. eng.*, **3**, 269–289 (1974).

21. B. LeDain-Muir and B. R. Baliga, 'Solution of three-dimensional convection-diffusion problems using tetrahedral elements and flow-oriented upwind interpolatin functions', *Numer. Heat Transfer*, **9**, 143–162 (1986).
22. S. F. McCormick, 'Multilevel adaptive methods for partial differential equations', in *Frontiers in Applied Mathematics*, vol. 6, SIAM, Philadelphia, 1989.
23. T. J. Barth, 'On unstructured grids and solvers', *Computational Fluid Dynamics*, Von Karman Institute Lecture Series, 1990–03, 1990.
24. J. G. Rice and R. J. Schnipke, 'An equal-order velocity-pressure formulation that does not exhibit spurious pressure modes', *Comp. methods. appl. mech. eng.*, **58**, 135–149 (1986).
25. M. Peric, R. Kessler, and G. Scheuerer, 'Comparison of finite-volume numerical methods with staggered and co-located grids', *Comput. Fluids*, **16**, 389–403 (1988).
26. S. Majumdar, 'Role of under-relaxation in momentum interpolation for calculation of flow with nonstaggered grids', *Numer. Heat Transfer*, **13**, 125–132 (1988).
27. B. R. Hutchinson and G. D. Raithby, 'A multigrid method based on the additive correction strategy', *Numer. Heat Transfer*, **9**, 511–537 (1986).
28. S. V. Patankar, D. K. Basu, and S. A. Alpay, 'Prediction of the three-dimensional velocity field of a deflected turbulent jet', *J. Fluids Engn.*, **99**, 758–762 (1977).
29. P. Chassang, J. George, A. Claria, and F. Sananes, 'Physical characteristics of subsoic jets in a cross stream', *J. Fluid Mech.*, **62** Part 1, 41–64 (1974).
30. Dimitriadis, K. P., Computation of three-dimensional turbulent flow in a non-orthogonal duct junction, Ph. D. Thesis, Manchester, 1986.